Ionisation Structure in Accretion Shocks with a Composite Cooling Function

Kinwah Wu[1,2], Mark Cropper[2] & Gavin Ramsay[2]

[1] *Research Centre for Theoretical Astrophysics, School of Physics A28, University of Sydney, NSW 2006, Australia*
[2] *Mullard Space Science Laboratory, University College London, Holmbury St. Mary, Dorking, Surrey RH5 6NT*

ABSTRACT

We have investigated the ionisation structure of the post-shock regions of magnetic cataclysmic variables using an analytic density and temperature structure model in which effects due to bremsstrahlung and cyclotron cooling are considered. We find that in the majority of the shock-heated region where H- and He-like lines of the heavy elements are emitted, the collisional-ionisation and corona-condition approximations are justified. We have calculated the line emissivity and ionisation profiles for Iron as a function of height within the post-shock flow. For low-mass white dwarfs, line emission takes place near the shock. For high-mass white dwarfs, most of the line emission takes place in regions well below the shock and hence it is less sensitive to the shock temperature. Thus, the line ratios are useful to determine the white-dwarf masses for the low-mass white dwarfs, but the method is less reliable when the white dwarfs are massive. Line spectra can, however, be used to map the hydrodynamic structure of the post-shock accretion flow.

Key words: accretion — shock waves — X-rays: stars — stars: white dwarfs – methods: data analysis

1 INTRODUCTION

When a supersonic accretion flow abruptly becomes subsonic near the surface of a compact star, a stand-off shock is formed. For the white dwarfs in magnetic cataclysmic variables (mCVs) (see Warner 1995), the accretion-shock temperature $T_s = 3\, G\mu m_H M_w/8kR_w$ (if $x_s << R_w$), where G is the gravitational constant, k the Boltzmann constant, m_H the hydrogen mass, μ the mean molecular weight of the gas, x_s the shock height, M_w the mass of the white dwarf and R_w the radius of the white dwarf. (Typically, $T_s \sim 10^8$ K.) As T_s depends on M_w and R_w, and is insensitive to other orbital parameters, the white-dwarf mass can be determined if T_s is measured (Rothschild et al. 1981; Kylafis & Lamb 1982; Ishida 1991; Fujimoto & Ishida 1997; Cropper, Ramsay & Wu 1998).

The distance from the shock front to the white-dwarf surface (i.e. the shock height) and the structure of the shock-heated emission region depends not only by T_s but also the cooling processes. For mCVs, bremsstrahlung and cyclotron cooling are the most important. When the accretion rate of the system is high ($\gtrsim 10^{16}$ g s^{-1}) and the white-dwarf magnetic field is weak (~ 1 MG), bremsstrahlung cooling usually dominates. If the accretion rate is low ($\lesssim 10^{16}$ g s^{-1}) and the magnetic field is strong ($\gtrsim 10$ MG), then cyclotron cool-

ing is the dominant process, at least near the shock (Lamb & Masters 1979; King & Lasota 1979). Line cooling is generally unimportant, except at the bottom of the post-shock region, where the electron temperature T_e falls well below 10^7 K (e.g. Kato 1976; Mewe, Gronenschild & van den Oord 1985).

It is straightforward to calculate the post-shock accretion flow with only optically thin bremsstrahlung cooling (see e.g. Aizu 1973; Chevalier & Imamura 1982). The inclusion of cyclotron cooling complicates the calculations because of large opacity effects. An exact treatment of cyclotron cooling requires the solving of the radiative-transfer and hydrodynamic equations simultaneously, and it is unlikely that simple analytic solutions can be obtained. However, for parameters typical of mCVs, the total cooling process can be roughly approximated by a composite cooling function with power laws of density and temperature (Langer, Chanmugam & Shaviv 1982; Wu 1994; Wu, Chanmugam & Shaviv 1994). With this composite cooling function, the hydrodynamic equations governing the post-shock flow can be solved, yielding a closed-form solution. With the density and temperature structures of the emission region specified, the X-ray emission from the system can be calculated. (See Wu 2000, for a review of accretion shocks in mCVs.)

X-rays emitted from regions in which both cyclotron and bremsstrahlung cooling are important are generally softer than those from regions with bremsstrahlung cooling only. Moreover, the spectra of the cyclotron-bremsstrahlung cooling shocks are richer in emission lines (Cropper, Ramsay & Wu 1998; Tennant et al. 1998). Emission lines can also be used to diagnose the density and temperature structures of the shock-heated region (see Fujimoto & Ishida 1995; Ezuka & Ishida 1999). The grating instruments on board the current X-ray satellites *XMM-Newton* and *Chandra* can easily resolve many of the emission lines in the ~ 1 keV range. With the spectral resolution of these satellites we will be able to measure the accretion flow very close to the white-dwarf surface.

From the X-ray continuum, the shock temperature can be determined, and hence the white-dwarf mass (e.g. Ishida 1991; Cropper, Ramsay & Wu 1998; Ramsay 2000; Beardmore, Osborne & Hellier 2000). In analysing X-ray data, model continua spectra are fitted to the data in order to determine the system parameters. As noted above, numerical calculations with exact treatment of cyclotron cooling will in principle produce more accurate model spectra, but its heavy demand on computation time makes it impractical in most situations. Semi-analytic methods that can yield reasonably accurate results are therefore more useful in the data analysis to extract system parameters, such as the shock temperature. In this study we investigate the ionisation structures and the line emission of the post-shock emission regions of mCVs in terms of the analytic treatment of Wu (1994) and Wu, Chanmugam & Shaviv (1994). We ignore the effects of gravity over the height of the shock (e.g. Cropper et al. 1999) and unequal ion and electron temperatures (e.g. Imamura et al. 1987; Saxton 1999; Saxton & Wu 1999).

2   STRUCTURED SHOCK-HEATED REGIONS

The ionisation of the elements in the post-shock flow in mCVs is generally caused by X-ray irradiation or collisions. The electron transitions between the K-, L-shells and the outer shells are the major processes in producing the keV emission lines. The strength of the lines are therefore determined by the temperature, density, and the ionisation structures of the emission region.

The electron temperature at the accretion shock is $\sim 10^8$ K. This temperature is sufficient to completely ionise the elements such as Argon, Silicon, Sulphur, Aluminium or Calcium through electron collisions. Iron can be ionised to the highest ionisation states: Fe XXVI and Fe XXVII.

The ionisation due to irradiation can be described by the ionisation parameter, which is defined as $\xi = L_{\rm x}/n_{\rm H} r^2$ (Kallman & McCray 1982). (Here, $L_{\rm x}$ is the luminosity of the irradiation, $n_{\rm H}$ is the number density of hydrogen, and r is the characteristic size of the plasma.) In the shock-heated region of mCVs, $L_{\rm x} \sim 10^{31} - 10^{33}$ erg s^{-1}, $n_{\rm H} \sim 10^{15} - 10^{16}$ cm^{-3}, and $r \sim 10^8$ cm and the ionisation parameter is $\lesssim 10^2$. The corresponding ionisation states of Iron are Fe XX or lower (Makishima 1986).

Therefore, in the shock-heated regions of mCVs collisional ionisation is the major process producing the keV

emission lines. Photo-ionisation is important only in the cooler and less dense pre-shock accretion stream.

2.1   Collisional ionisation equilibrium

For $T \sim 10^7 - 10^8$ K, collisional ionisation equilibrium can be attained when $n_{\rm e} t > 10^{12}$ cm^{-3}s, where $n_{\rm e}$ is the electron number density and t is the time spent by the ions in the plasma (Gorenstein, Harnden & Tucker 1974; Masai 1984). For a white dwarf with a specific accretion rate $\dot{m}$, the local value of $n_{\rm e} t$ at ζ (the distance normalised to the shock height $x_{\rm s}$) is

$$
\begin{aligned}
\left[n_{\rm e} t\right]_\zeta &\approx \left| \frac{\dot{m}}{m_{\rm H} v} \int_v^{v_{\rm ff}/4} \frac{dv'}{v'} \frac{dx}{dv'} \right| \\
&= \frac{x_{\rm s} R_{\rm w} \dot{m}}{2 G M_{\rm w} m_{\rm H}} \frac{1}{\tau} \int_\tau^{1/4} \frac{d\tau'}{\tau'} \left(\frac{d\zeta}{d\tau'} \right) ,
\end{aligned}
\tag{1}
$$

where $\tau = -v/v_{\rm ff}$ is the dimensionless velocity, and $v_{\rm ff}$ is the free-fall velocity at the white-dwarf surface.

To evaluate the integral in the above equation we consider the inverted velocity profile of the accretion flow given in the hydrodynamic model of Wu (1994) (see Cropper, Ramsay & Wu 1998 for typographical corrections):

$$
\frac{d\zeta}{d\tau} = \frac{2 v_{ff}^2}{x_{\rm s} A \rho_{\rm s}} \frac{\tau^2 (5 - 8\tau)}{\sqrt{\tau(1-\tau)}} K(\tau) ,
\tag{2}
$$

where $K(\tau) = 1 + 3^{-\alpha} 4^{\alpha+\beta} \epsilon_{\rm s} (1-\tau)^\alpha \tau^\beta$ (with $\alpha \approx 2$ and $\beta \approx 3.85$ appropriate for cyclotron cooling), $\rho_{\rm s}$ is the density at the shock surface, $\epsilon_{\rm s}$ is the ratio of the bremsstrahlung-cooling time-scale to the cyclotron-cooling time-scale at the shock, and $A = 3.9 \times 10^{16}$ in c.g.s. units. The shock-height $x_{\rm s}$ can be obtained by a direct integration of the inverted velocity profile, i.e.,

$$
x_{\rm s} = \frac{2 v_{\rm ff}^2}{A \rho_{\rm s}} \int_0^{1/4} d\tau \frac{\tau^2 (5 - 8\tau)}{\sqrt{\tau(1-\tau)}} K(\tau) .
\tag{3}
$$

In this formulation, the hydrodynamic variables, such as density ρ, pressure P and temperature T, are proportional to $1/\tau$, $(1-\tau)$, and $\tau(1-\tau)$ respectively (see Wu 1994; Wu, Chanmugam & Shaviv 1994).

By combining Equations (1) and (3), this yields

$$
\left[n_{\rm e} t\right]_\zeta \approx 2.2 \times 10^{16} \ F_1(\zeta; \epsilon_{\rm s})
$$

$$
\times \left(\frac{M_{\rm w}}{M_\odot} \right)^{1/2} \left(\frac{R_{\rm w}}{5 \times 10^8 \ {\rm cm}} \right)^{-1/2} {\rm cm}^{-3} {\rm s} ,
\tag{4}
$$

where

$$
F_1(\zeta; \epsilon_{\rm s}) = \frac{1}{\tau(\zeta)} \int_{\tau(\zeta)}^{1/4} d\tau' \frac{\tau'(5 - 8\tau')}{\sqrt{\tau'(1-\tau')}} K(\tau') .
\tag{5}
$$

As $t \sim x_{\rm s}/v_{\rm ff} \sim n_{\rm e}^{-1} \min(1, \epsilon_{\rm s}^{-1})$, when $\epsilon_{\rm s}$ is specified $[n_{\rm e} t]_\zeta$ does not explicitly depend on $\dot{m}$ (see Equation 4). In Figure 1, we show $2.2 \times 10^4 \ F_1(\zeta; \epsilon_{\rm s})$ as a function of $(1-\zeta)$, the distance from the shock surface. When $2.2 \times 10^4 \ F_1(\zeta; \epsilon_{\rm s}) > 1$, the accreting matter is in collisional ionisation equilibrium. Figure 1 shows that except in a very thin layer near the shock front itself, collisional ionisation equilibrium is reached in the post-shock region for the range of $\epsilon_{\rm s}$ of interest.
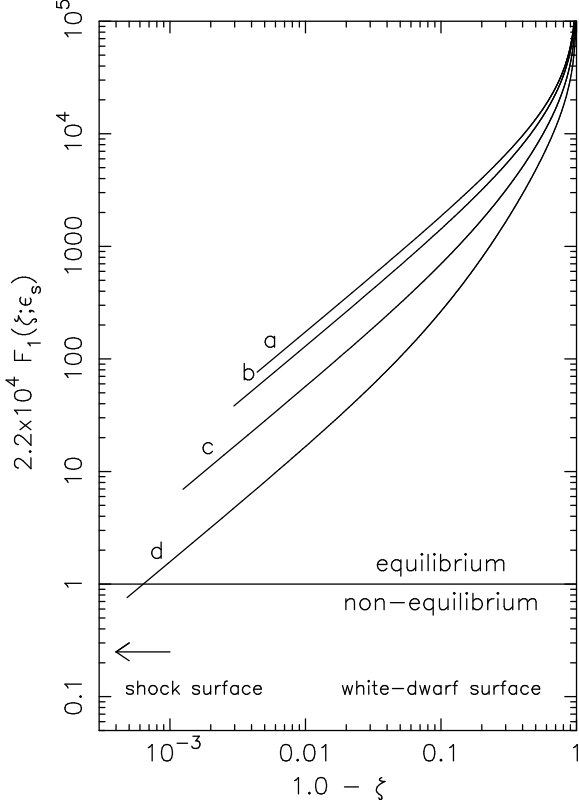
Figure 1. The quantity $2.2 \times 10^4 F_1(\zeta; \epsilon_s)$ as a function of $(1-\zeta)$, the normalised distance from the shock surface. The plasma is in collisional equilibrium if $2.2 \times 10^4 F_1(\zeta; \epsilon_s) > 1$. Curves a, b, c and d correspond to $\epsilon_s = 0$, 1, 10 and 100 respectively.

Figure 2. $5 \times 10^6 F_2(\zeta; \epsilon_s, Z)$ as a function of ζ, the normalised height from the white-dwarf surface, for Iron ($Z = 26$). For the solid curves $M_w = 1.0 M_\odot$ and $R_w = 5.53 \times 10^8$ cm; and for the dotted curves, $M_w = 0.5 M_\odot$ and $R_w = 9.61 \times 10^8$ cm. In each set of the curves, the corresponding ϵ_s are 0, 1, 10 and 100 (from top to bottom respectively). The horizontal line represents $F_2(\zeta; \epsilon_s, Z) = 2.0 \times 10^{-7}$, above which the approximation of corona condition is applicable.

2.2 Ionisation balance

The ionisation balance is determined by the excitation and de-excitation rates of the corresponding ionisation states. As the rate coefficients may depend on the optical depth, it is generally required to solve the coupled population rate and radiative-transfer equations to obtain the population of the ionisation states (Bates, Kingston & McWhirter 1962; Castor 1993). However, if the electron number density is sufficiently low that the radiative-transfer effects are unimportant, the ionisation balance can be calculated using the corona-condition approximation. In the other extreme, if the electron number density is sufficiently high such that the plasma is able to attain local thermal equilibrium (LTE), the population can then be determined by the Saha equation.

For the corona condition to hold, it requires the gas to be in collisional equilibrium and a direct coupling of the heat input to the ions and the free electrons. It also requires the density of the plasma to be sufficiently low such that most ions are in ground states, and the line (and continuum) emission to be optically thin (Elwert 1952; Mewe 1990; Kahn & Liedahl 1991).

For ions with a bared nuclear charge Z, the corona condition is satisfied if $n_e \lesssim 4 \times 10^4 Z^2 T_e^2$ cm^{-3} (Wilson 1962; Mewe 1990). As n_e and T_e scale with $1/\tau$ and $\tau(1-\tau)$,
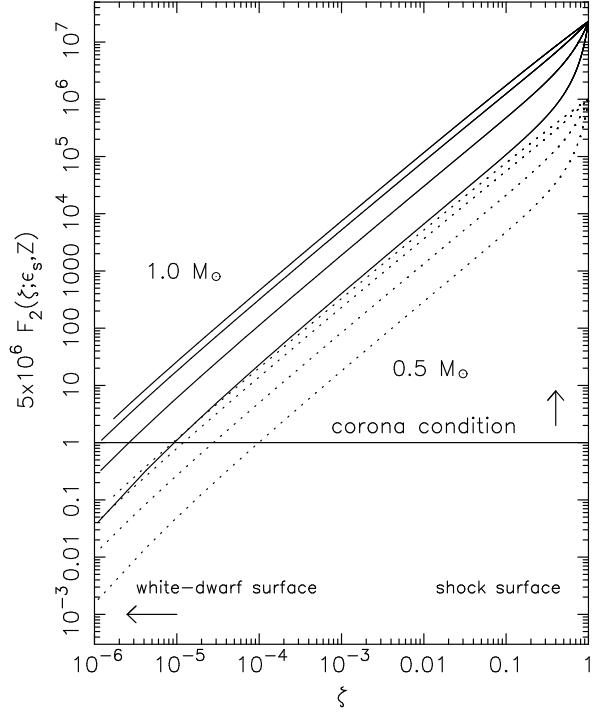
where τ is the dimensionless velocity (see §2.1), we can define a quantity

$$F_2(\zeta; \epsilon_s; Z) = Z^2 \tau(\zeta)^3 [1 - \tau(\zeta)]^2 \left(\frac{\mu}{0.5}\right)^2 \left(\frac{\dot{m}}{1 \text{ g s}^{-1}}\right)^{-1}$$

$$\times \left(\frac{M_w}{M_\odot}\right)^{5/2} \left(\frac{R_w}{5 \times 10^8 \text{ cm}}\right)^{-5/2} . \quad (6)$$

The corona-condition criterion is then equivalent to require $F_2(\zeta; \epsilon_s; Z) \gtrsim 2 \times 10^{-7}$.

In Figure 2 we show the profile of the function $[5 \times 10^6 F_2(\zeta; \epsilon_s, Z)]$ in the shock-heated regions of accreting magnetic white dwarfs for various parameters. It can be seen that for white dwarfs with $M_w = 1$ M$_\odot$ and $\dot{m} = 1$ g s^{-1}, the corona condition is satisfied when the height $\zeta > 10^{-5}$. For white dwarfs with $M_w = 0.5$ M$_\odot$, $\zeta > 10^{-4}$. The corona-condition approximation is not applicable at the very bottom of the shock-heated region, where the electron number density is high and the temperature is low.

A plasma is in LTE when $n_e \gtrsim 1.4 \times 10^{15} Z^6 T^{1/2}$ cm^{-3} (Wilson 1962). In terms of the velocity profile of the post-

shock accretion flow and white-dwarf parameters, it requires

$$1 \gtrsim 9.7 \times 10^4 Z^6 \tau(\zeta)^{3/2} [1 - \tau(\zeta)]^{1/2} \left(\frac{\mu}{0.5} \right)^{1/2}$$

$$\times \left(\frac{\dot{m}}{1 \text{ g s}^{-1}} \right)^{-1} \left(\frac{M_{\rm w}}{\rm M_\odot} \right) \left(\frac{R_{\rm w}}{5 \times 10^8 \text{ cm}} \right)^{-1}. \qquad (7)$$

For Iron, $Z = 26$. LTE implies $\tau \lesssim 10^{-9}$, corresponding to $v \lesssim 1 \text{ cm s}^{-1}$. Thus, LTE is applicable for the very base of the post-shock flow only.

2.3 Ionisation profiles

Ionisation-balance calculations in the approximation of corona condition have been carried out by many authors (e.g. Jordan 1969; Jacobs et al. 1977; Raymond & Smith 1977; Mewe & Gronenschild 1981; Arnaud & Rothenflug 1985; Mewe, Gronenschild & van den Oord 1985). The results of the calculations are usually presented in terms of $n_{\rm z}/\sum_{\rm z} n_{\rm z}$ (the relative ion concentration) as a function of $T_{\rm e}$ (the electron temperature). With the local value for the electron number density, the electron temperature and the abundance of the elements specified, the results of these ionisation balance calculations can be readily used to determine the concentration of the ion species.

The temperature of the accretion shock in mCVs is typically $\sim 10^8$ K, which is sufficient to ionise Iron in the shock-heated region to its higher ionisation states. As only the most populous ion species would make significant contribution to the emission, in this study we only consider the four most highly ionisation states, Fe XXVII (Fe^{26+}), Fe XXVI (Fe^{25+}), Fe XXV (Fe^{24+}) and Fe XXIV (Fe^{23+}). Also, we restrict the emission region of interest to be $\zeta > 10^{-4}$, where the corona condition is satisfied.

We first determine the local ionisation by interpolating the results from the ionisation balance calculations of Arnaud & Rothenflug (1985) and then use it to calculate the profiles of the relative concentration of the ion species in the shock-heated region. Two representative cases are considered, with the white-dwarf masses 1.0 and 0.5 $\rm M_\odot$ respectively for each case. (We have assumed the Nauenberg (1972) mass-radius in the calculations.) The parameter $\epsilon_{\rm s}$ is chosen to be 0, 1, 10 and 100. This covers the range of parameters appropriate for most mCVs (see Wu, Chanmugam & Shaviv 1994).

In Figures 3 and 4 we show the relative ion concentrations of Iron as a function of the height above the white-dwarf surface for the 1.0-$\rm M_\odot$ and 0.5-$\rm M_\odot$ white dwarfs respectively. The normalisation is such that the total concentration is 1.0 at the shock surface ($\zeta = 1$). As the density (and the electron number density $n_{\rm e}$) increases when ζ decreases, the peak concentration of each ion species is always ≥ 1.0. Since the temperature and density in the post-shock region are monotonic functions of ζ (if the electrons and ions have the same temperature and the variation of gravity with height is negligible), when the temperature is specified, the density is uniquely determined. In ionisation equilibrium, the peak concentration of the ion species depends only on $T_{\rm e}$. Thus, for a fixed white-dwarf mass, the peak concentrations occur at the same $T_{\rm e}$ and $n_{\rm e}$, in spite of the different values of $\epsilon_{\rm s}$.
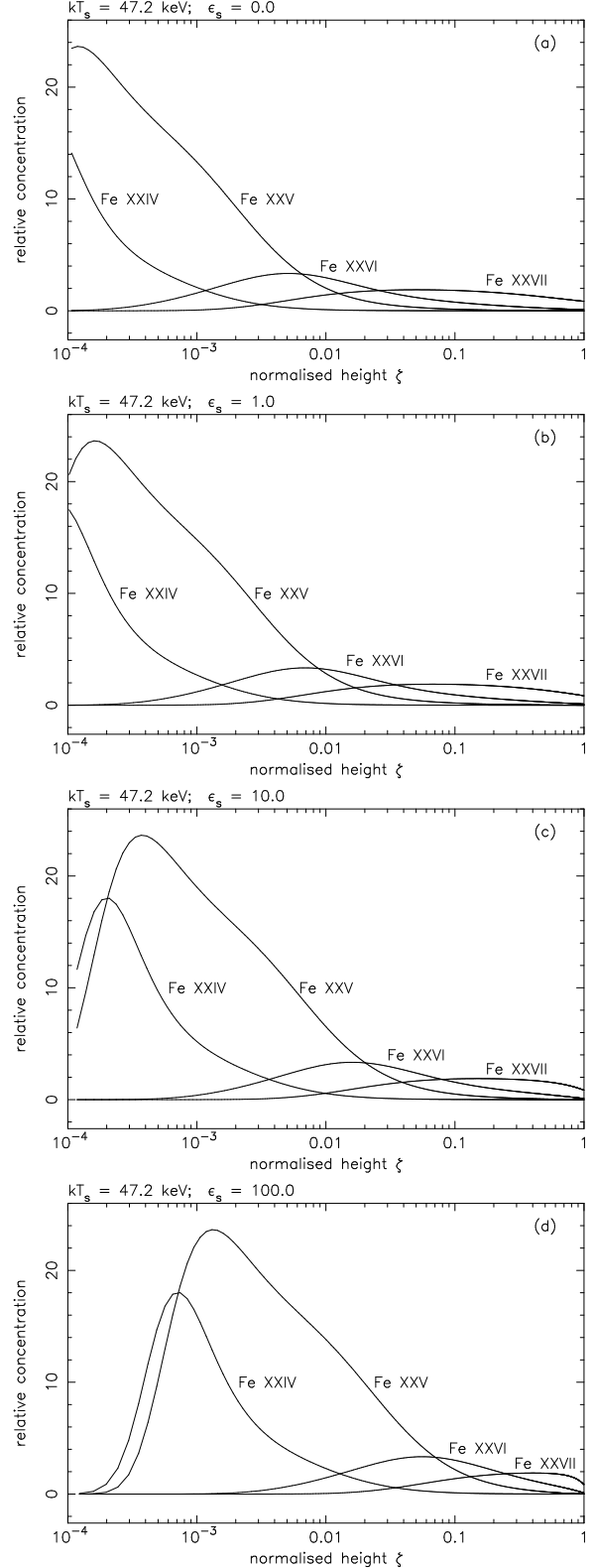

Figure 3. The ionisation profile of Fe XXVII, Fe XXVI, Fe XXV and Fe XXIV in the shock-heated emission region of a 1.0-$\rm M_\odot$ white dwarf. The effects of cyclotron cooling increases from the top to the bottom panels (from panel (a) to panel (d) respectively), and the corresponding parameters are $\epsilon_{\rm s} = 0$, 1, 10 and 100. The surface of the white dwarf is at $\zeta = 0$, and the shock surface is at $\zeta = 1$.
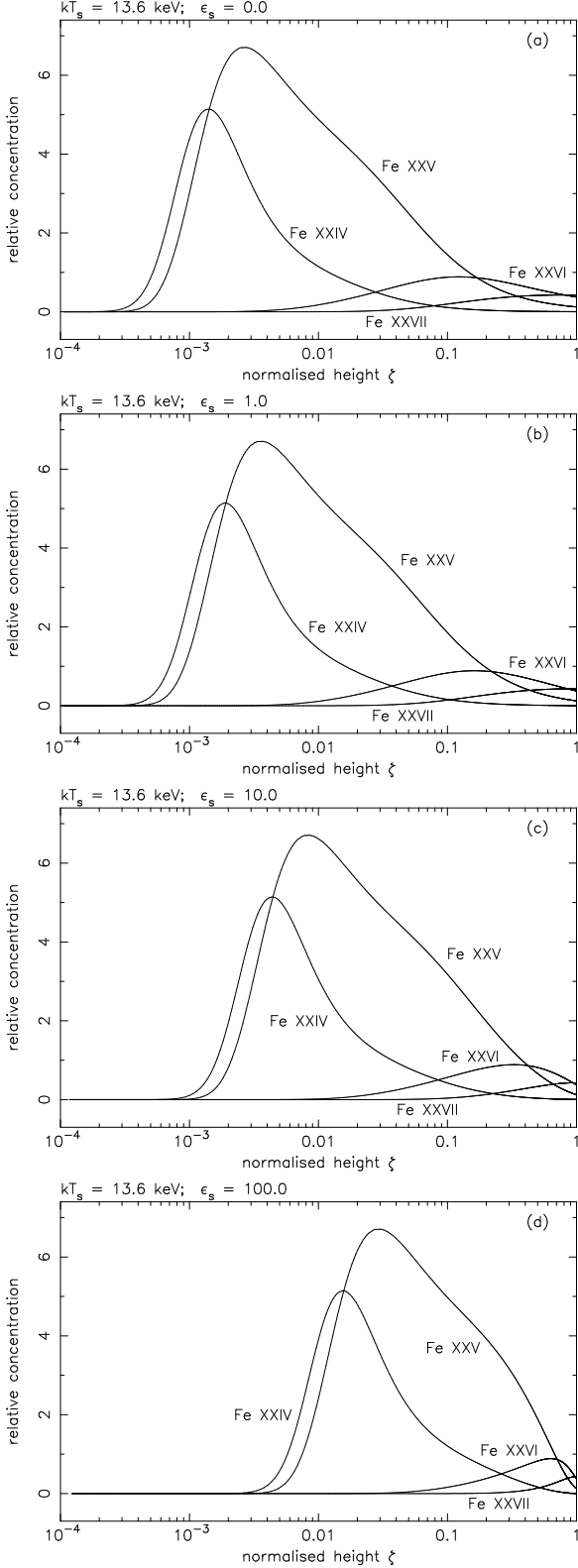
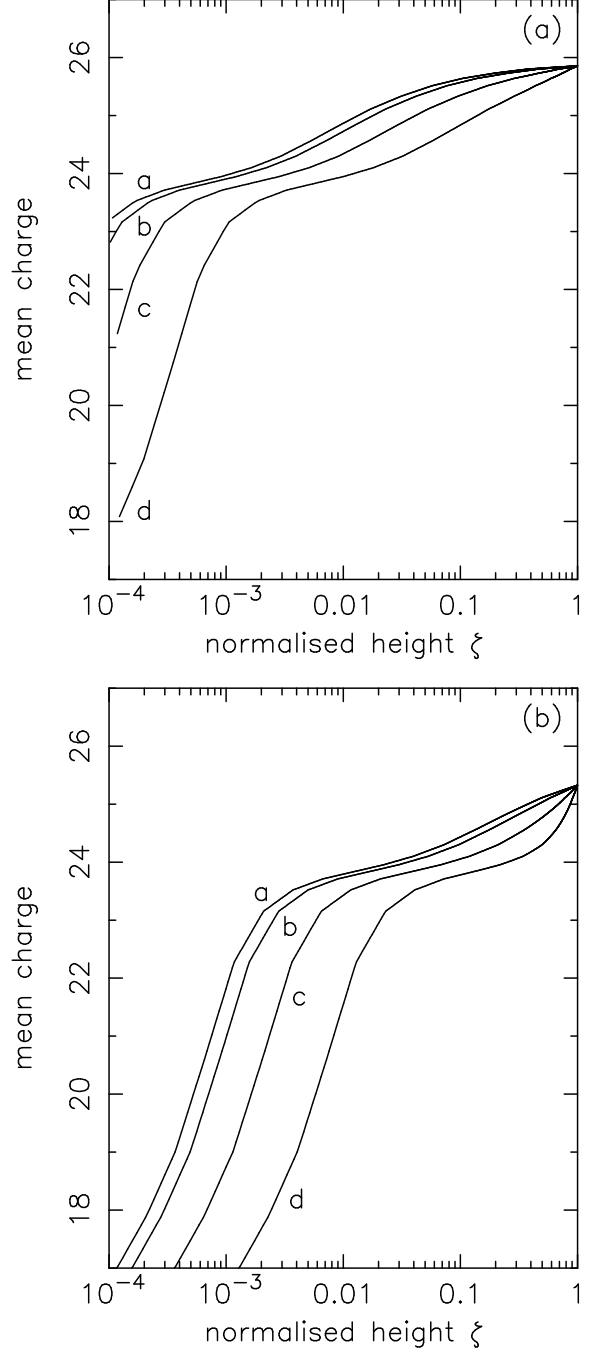**Figure 4.** Same as Fig. 3 for a white dwarf with 0.5 M$_\odot$.

Figure 5. he mean charge profile of Iron in the shock-heated region for (a) $M_{\rm w} = 1.0 {\rm M_\odot}$; and (b) for $M_{\rm w} = 0.5 {\rm M_\odot}$. Curves a, b, c and d correspond to $\epsilon_{\rm s} = 0$, 1, 10 and 100 respectively.

As shown in Fig 3, Fe XXVII dominates in most of the shock-heated region of the 1.0-M$_\odot$ white dwarf with $\epsilon_{\rm s} = 0$. The lower ionisation states are important only near the low-temperature bottom of the post-shock region. For larger $\epsilon_{\rm s}$, the emission region is cooler, and so the lower ionised species becomes more abundant. When $\epsilon_{\rm s} = 100$, the relative concentration of Fe XXVI is higher than that of Fe XXVII in the region where $\zeta \sim 0.1 - 0.3$. However, as a whole, Fe XXVII still dominates in the post-shock region. For a 0.5-M$_\odot$ white dwarf, the shock temperature $kT_{\rm s} \approx 13.6$ keV, which is
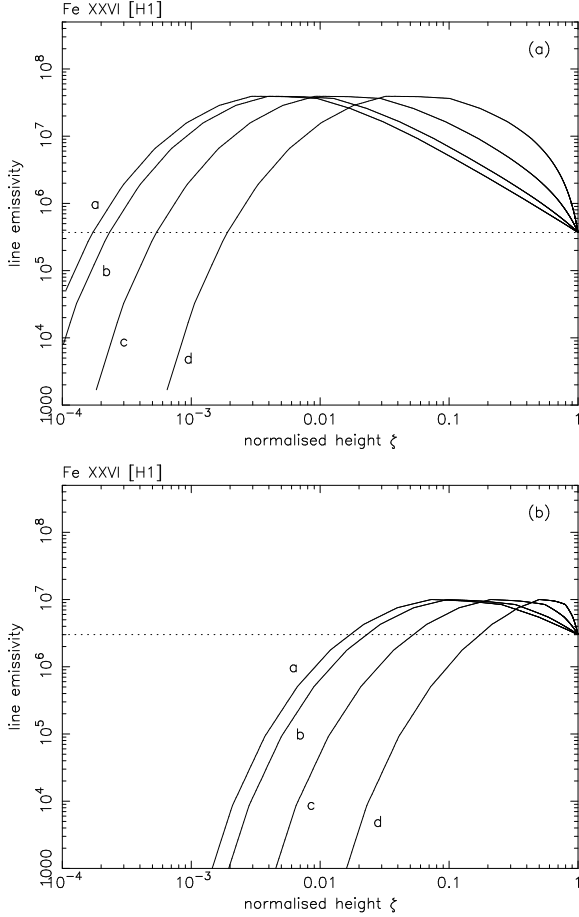
Figure 6. The emissivity (in erg cm^{-3} s^{-1}) profile of the Fe XXVI Lyman-α (1s ^{2}S – 2p ^{2}P) transition for a white dwarf with a mass of 1.0 M$_\odot$ (upper panel) and 0.5 M$_\odot$ (lower panel). The specific accretion rate is $\dot{m} = 1$ g cm^{-2} s^{-1}. Curves a, b, c and d correspond to $\epsilon_\mathrm{s} = 0$, 1, 10 and 100 respectively. For comparison, we also show in dotted line the line emissivity of emission regions with constant electron temperature and number density the same as the values at the shock of the structured emission regions that we consider.

insufficient to completely ionise all the Iron to Fe XXVII. For $\epsilon_\mathrm{s} \lesssim 1$ the dominant species is Fe XXVI, and for $\epsilon_\mathrm{s} \gtrsim 10$, Fe XXV. As in the previous case, the lower ionisation states becomes more important at the bottom of the post-shock region.

In Figure 5, we show the mean charge ($\bar{z}$) profiles. For the 1.0-M$_\odot$ white dwarfs, $\bar{z} \approx 25.8$ at the shock surface, which implies that Fe XXVII is the most abundant ion. As ζ decreases, $\bar{z}$ first decreases slowly to ≈ 24 and then falls more rapidly afterwards. For $\epsilon_\mathrm{s} = 0$ (bremsstrahlung cooling only), $\bar{z} \approx 23.2$ at $\zeta = 10^{-4}$; while for $\epsilon_\mathrm{s} = 100$ (cyclotron cooling dominated), $\bar{z} \approx 18$ at $\zeta = 10^{-4}$. For the 0.5-M$_\odot$ white dwarfs, $\bar{z} \approx 25.3$ (i.e. Fe XXVI dominates) at $\zeta = 1.0$. Similarly to the 1.0-M$_\odot$ case, $\bar{z}$ decreases slowly with ζ until it reaches ≈ 24 and then rapidly afterwards. For $\epsilon_\mathrm{s} = 0$, $\bar{z} = 17$ at $\zeta \sim 10^{-4}$; and for $\epsilon_\mathrm{s} = 100$, $\bar{z} = 17$ at $\zeta \sim 10^{-3}$.
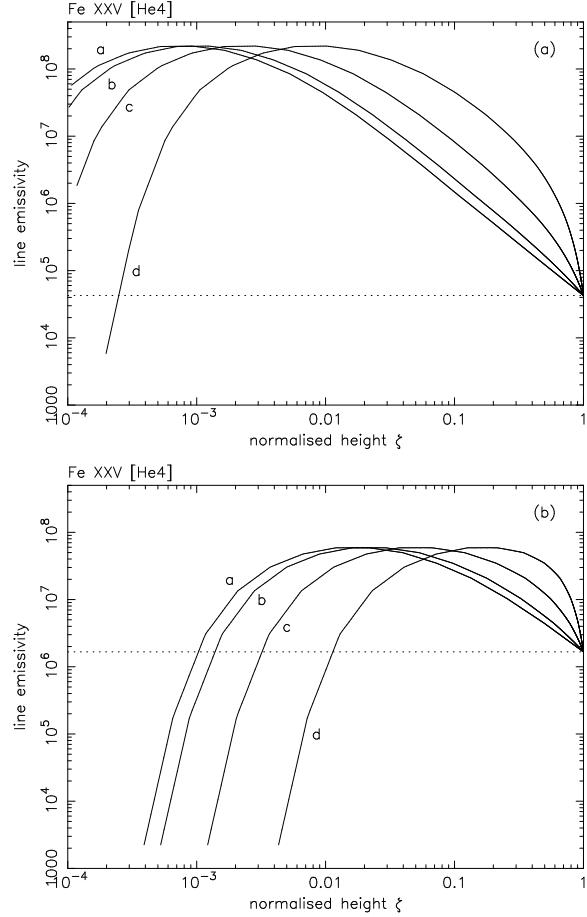

Figure 7. Same as Fig. 6 for the Fe XXV He4 (1s^2 ^{1}S – 1s2p ^{1}P) transition.

2.4   Line emissivity profile

In Figures 6, 7, 8 and 9, the line emissivity of the Fe XXVI Lyman-α (1s ^{2}S – 2p ^{2}P), Fe XXV He4 (1s^2 ^{1}S – 1s2p ^{1}P), Fe XXV He5 (1s^2 ^{1}S – 1s2p ^{3}P), and Fe XXV He6 (1s^2 ^{1}S – 1s2p ^{3}S) lines are shown. The corresponding line centre energies of these lines are 6.93, 6.70, 6.68 and 6.64 keV. In calculating the emissivity we have interpolated the table of line power given in Mewe, Gronenschild & van den Oord (1985). The electron number density that we assume corresponds to an specific accretion rate of $\dot{m} = 1$ g cm^{-2} s^{-1}.

When the white-dwarf mass and the accretion rate are fixed, the emissivity of an emission line is the same at the shock for all ϵ_s. As ϵ_s increases, cyclotron cooling becomes more efficient. As the electron temperature of the shock-heated region is lowered, the lower ionised species becomes more significant. As a result, the emissivities of the Fe XXVI and Fe XXV lines all peak at larger ζ for larger ϵ_s (Fig. 10).

3   DISCUSSION

3.1   White-dwarf mass determination

When the local emissivity $P_\mathrm{l}(\zeta; T_\mathrm{s}, \epsilon_\mathrm{s}, z_\mathrm{i})$ of an emission line z_i is specified, the intensity of the line is simply the sum of contribution from all zones in the emission region, i.e.,

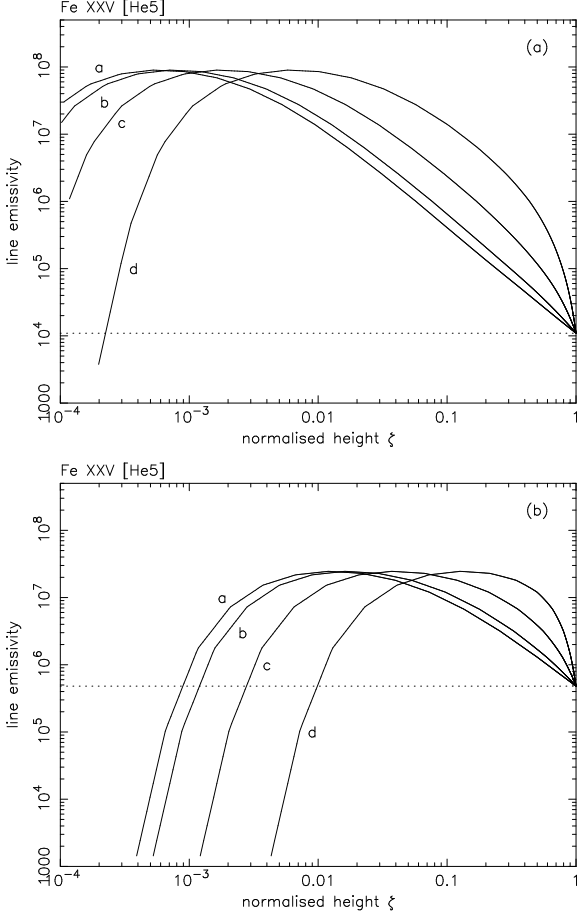**Figure 8.** Same as Fig. 6 for the Fe XXV He5 ($1s^2$ ^{1}S – 1s2p ^{3}P) transition.

Figure 9. Same as Fig. 6 for the Fe XXV He6 ($1s^2$ ^{1}S – 1s2p ^{3}S) transition.

$$I(z_i) \approx \frac{x_s S}{4\pi D^2} A(Z) \int_{\Delta_i}^1 d\zeta P_l(\zeta; T_s, \epsilon_s, z_i) , \qquad (8)$$

where $A(Z)$ is the abundance of the element that give rise to the emission line z_i, Δ_i the height above the white-dwarf surface at which the emission becomes optically thick, S the cross-section area of the emission region, and D is the distance of the source. In terms of the temperature gradient $dT/d\zeta$,

$$I(z_i) = \frac{x_s S}{4\pi D^2} A(Z) T_s \int_{T_{\Delta_i}}^{T_s} dT \frac{d\zeta}{dT} P_l(\zeta; T_s, \epsilon_s, z_i) , \qquad (9)$$

where T_{Δ_i} is the temperature at Δ_i. The ratio of the intensities of two emission lines z_i and z_j of the same element Z are therefore

$$R(z_i, z_j; T_s, \epsilon_s, \Delta_i, \Delta_j) = \frac{\int_{T_{\Delta_i}}^{T_s} dT \frac{d\zeta}{dT} P_l(\zeta; T_s, \epsilon_s, z_i)}{\int_{T_{\Delta_j}}^{T_s} dT \frac{d\zeta}{dT} P_l(\zeta; T_s, \epsilon_s, z_j)} . \qquad (10)$$

As the line-intensity ratio is a function of ϵ_s, T_s, T_{Δ_i} and T_{Δ_j} only, one may use the observed line intensity ratio to constrain these parameters.

Fujimoto (1996) and Fujimoto & Ishida (1995, 1997) assumed that $T_{\Delta_j} = T_{\Delta_i} (= T_\Delta)$, and use the ratio of H- and He-like Fe Kα lines observed by *ASCA* to determine the shock T_s of the Intermediate Polar EX Hya. From the
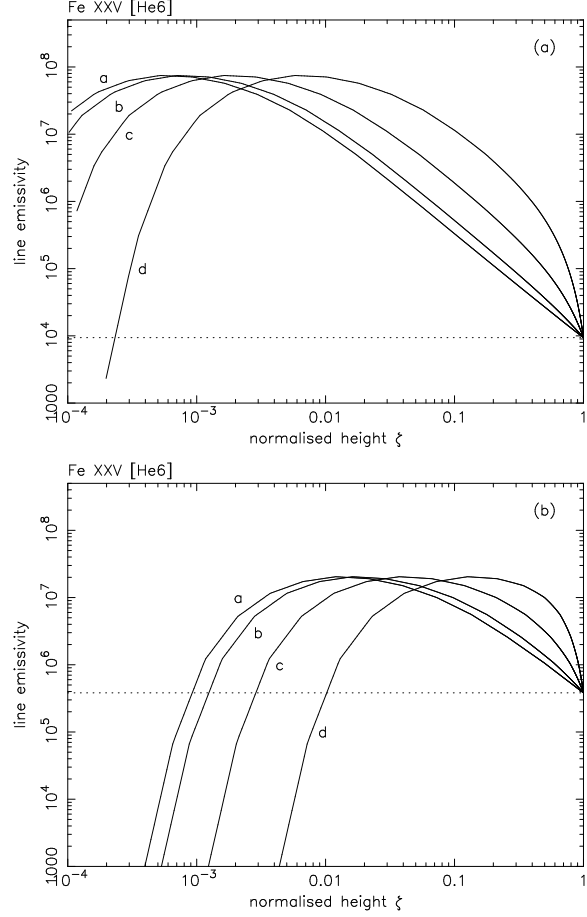
deduced shock temperature they obtained a white-dwarf mass of $0.48^{+0.10}_{-0.06}$ M$_\odot$. Using the same method, Hellier et al. (1996) deduced the white-dwarf mass of another Intermediate Polar AO Psc, giving $0.40^{+0.07}_{-0.11}$ M$_\odot$. These masses are generally in agreement with those determined by fitting the X-ray continuum using *Ginga* data (0.45 M$_\odot$ and 0.45 M$_\odot$ respectively for EX Hya and AO Psc) and *RXTE* data (0.44±0.03 M$_\odot$ and 0.60±0.03 M$_\odot$ respectively) (Cropper, Wu & Ramsay 1999; Ramsay 2000).

As the emissivity of the emission lines is sensitive to the temperature of the emission region, it is generally considered that white-dwarf masses can be accurately determined using spectral lines, and the line emission may provide better constraints to the white-dwarf masses than the continuum. However, an accurate measurement of the line strengths does not necessarily lead to an accurate determination of the *shock* temperature. The shock temperature can be deduced only if there are sufficient concentrations of ions that are responsible for the line emission at the shock. If the shock temperature is sufficiently high that the element is completely ionised at the shock, the strengths of its H- and He-like lines are insensitive to the shock temperature. These lines are now emitted from the cooler bottom of the post-shock region (cf. Fig. 10a and Fig. 10b). Thus, using Fe H- and He-like emission lines to determine white-dwarf mass is practical for the low-mass (~ 0.5 M$_\odot$) systems but not for massive
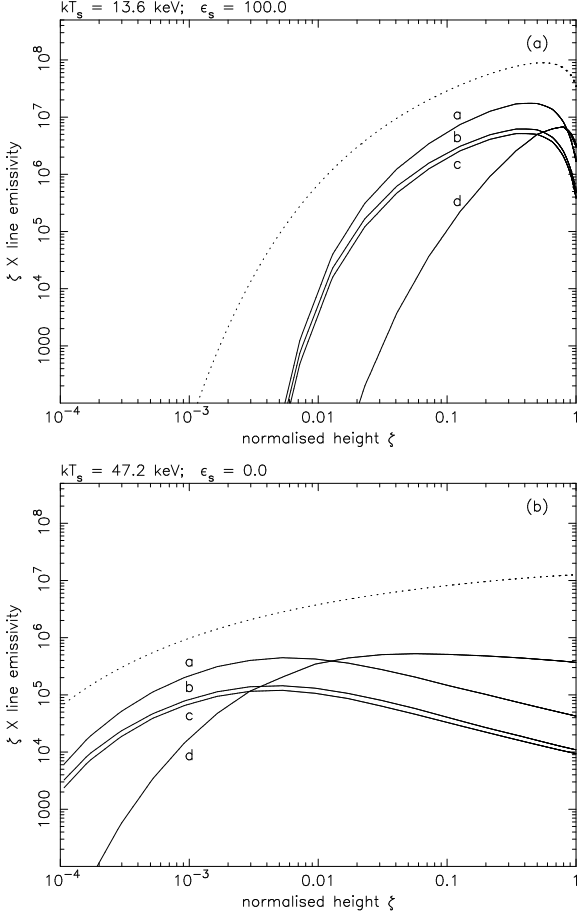
Figure 10. (a) The "$\zeta \times P_l$" emissivity profile of the continuum at 6.8 keV (dotted curve), the Fe XXV He4 line (curve a), the Fe XXV He5 line (curve b), the Fe XXV He6 line (curve c) and the Fe XXVI Lyman-α line (curve d) for a 0.5-M$_\odot$ strongly magnetised white dwarf with $\epsilon_s = 100$. (b) Same as (a) for a 1.0-M$_\odot$ white dwarf with $\epsilon_s = 0$.

white dwarfs (Wu 2000). Indeed, an attempt to constrain the white-dwarf masses of two more massive AM Her type systems, AM Her itself and BL Hyi, using this method was unsuccessful (Fujimoto & Ishida 1995). Although one may consider elements with higher ionisation potential, such as Nickel, the abundance of heavier elements in typical mCVs are generally low and unable to produce lines that are strong enough to be useful in typical observations. For instance in Figures 11, 12, 13 and 14 we show the strengths of the Fe and other lines in simulated *XMM-Newton* EPIC-PN and RGS spectra of accreting white dwarfs of different masses and cooling efficiencies. In these simulations we have used calibration files determined 7 months into flight and used exposures typical of *XMM-Newton* observations. Tennant et al. (1998) shows simulated spectra using the *Chandra* grating spectra.

3.2   Flow diagnosis

Because of the temperature and velocity stratification in the shock-heated region, the emission lines from different heights above the white-dwarf surface have different Doppler shifts.
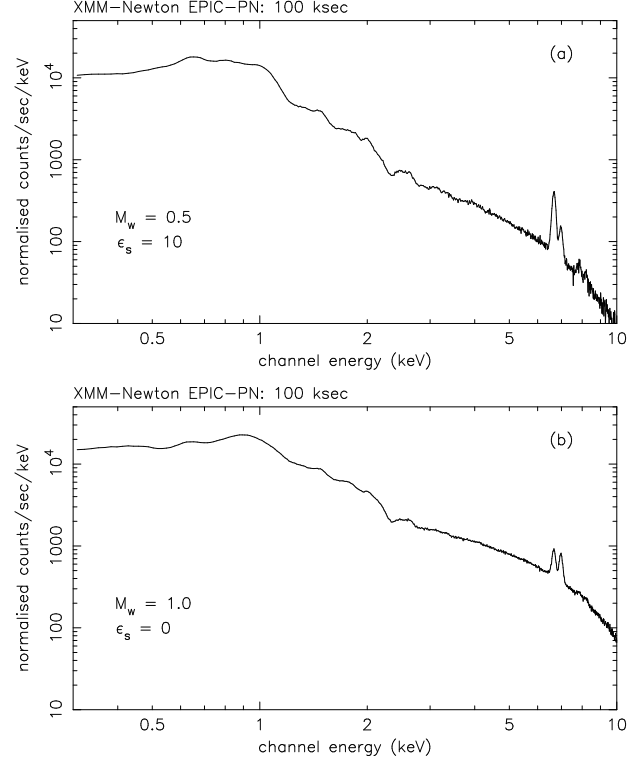

Figure 11. (a) Simulated *XMM-Newton* EPIC-PN spectra of a 0.5-M$_\odot$ white dwarf with substantial cyclotron cooling ($\epsilon_s = 10$) for a 100-ks exposure. We assume solar metal abundance. The flux is normalised to that of the observed flux of AM Her itself in the 2–10keV energy band ($\approx 7 \times 10^{-11}$ erg s^{-1} cm^{-2}) derived from *ASCA* data (0.5–10keV) (Ishida et al. 1997). (b) Same as (a) for a 1.0-M$_\odot$ white dwarf with no cyclotron cooling. In simulating the spectra we have used calibration files derived 7 months into the orbit of *XMM-Newton* and assume a medium filter.

A line can be emitted only if the temperature of the accretion matter allows the according electronic transition to occur, so one can infer the temperature and density of the region where the line is emitted. In addition the Doppler shift of the line centre energy can be measured, from which the line-of-sight velocity of the emitter can be deduced. Thus, by examining the different lines in a spectrum, one can obtain a relation between the flow velocity, temperature and density.

For a 1.0-M$_\odot$ white dwarf, the velocity of material at the accretion shock is about 2×10^8 cm s^{-1}. The centre energy of lines emitted from regions near the shock will have an energy shift of about 0.6%. As the white dwarf in a mCV revolves with the orbit and it also rotates, there is an additional velocity shift of about $2 - 3 \times 10^7$ cm s^{-1} for typical CV parameters. The white-dwarf rotational period and the binary orbital period are the same for typical AM Her type systems, and it allows us to subtract the velocity due to orbital motion and the white-dwarf rotation easily. Moreover, AM Her type systems do not have an accretion disc, and therefore the line spectra are emitted mainly from the hot shock-heated accretion matter near the white-dwarf surface. The Doppler shift of the emission lines is then only due to the bulk accretion flow, and they can be extracted as described above from the orbital phase-binned data.
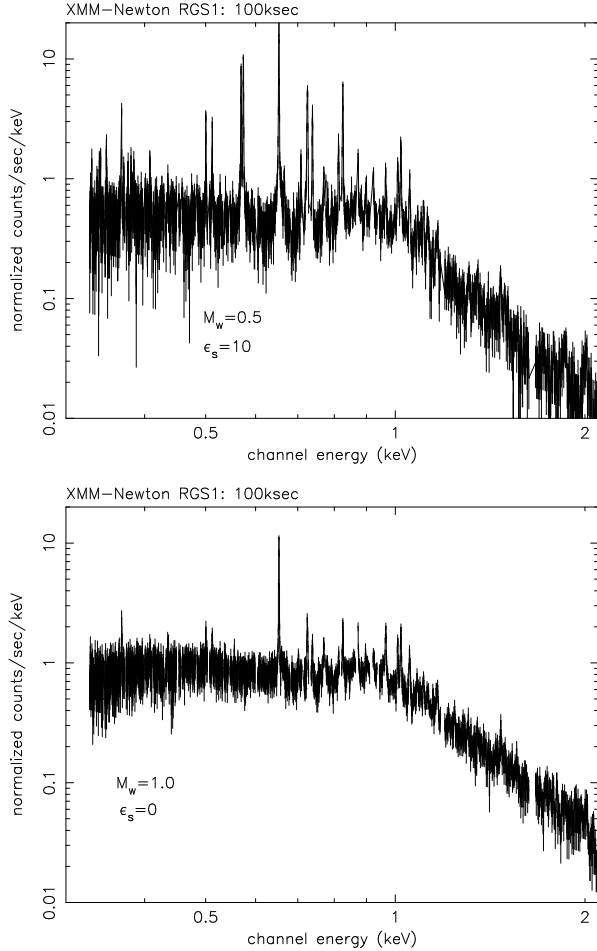
Figure 12. (a) Simulated *XMM-Newton* RGS spectra (0.3–2.1keV) of a 0.5-$M_\odot$ white dwarf with substantial cyclotron cooling ($\epsilon_s = a0$) for a 100-ks exposure. We assume solar metal abundance. The flux is normalised to the observed flux of the hard component of AM Her itself ($\approx 1.7 \times 10^{-11}$ erg s^{-1} cm^{-2}) determined from *ROSAT* data (0.1–2.4keV) (Ramsay et al. 1994). (b) Same as (a) for a 1.0-$M_\odot$ white dwarf with no cyclotron cooling. In simulating the spectra we have used calibration files derived 7 months into the orbit of *XMM-Newton*.

A line-centre energy resolution of 1 part in 10000 (achievable by *XMM-Newton* and *Chandra* at about 1 keV) will allow us to measure the accretion flow a few tens metres above the white-dwarf surface. As shown in Figures 13 and 14, the Fe complex and other lines are clearly resolved in the *XMM-Newton* simulated grating spectra for a 100-ksec observation. In the parallel study of Tennant et al. (1998), it was shown that an energy resolution of 0.1-eV can be achieved by the Medium Energy Gratings of *Chandra* for a single gaussian fit to a line of centre energy of 1 keV for about 200 photons in the lines. For a mCV of the X-ray brightness of the system AM Her itself, this requires an observation of about 100 ksec to detect this number photons in 1/10 of an orbital phase.

X-ray spectroscopy will therefore allow the flow velocity in these accreting systems to be measured directly. This diagnostic power cannot be achieved by optical spectroscopy, despite its better velocity resolution, as optical emission from the shock-heated material in mCVs is optically thick.

4 SUMMARY

We have investigated the ionisation structure and line emissivity profiles of the shock-heated emission regions of accreting white dwarfs in mCVs by means of an analytic model given in Wu (1994) and Wu, Chanmugam & Shaviv (1994). We have found that for Iron, the corona-condition approximation is generally satisfied in most of the shock-heated region where lines are emitted. Because of the temperature and density stratification in the shock-heated region, different lines are emitted from different heights above the white-dwarf surface. By measuring the Doppler shifts of the lines, one can obtain a relationship between the flow velocity, the temperature and the density of the emitting gas, thus providing a means to map the hydrodynamics of the post-shock accretion flow directly. Our study also indicates that using emission lines to determine white-dwarf masses is practical only for low-mass systems. For massive systems, the abundant elements such as Fe are completely ionised at the shock and so their line emission is insensitive to the shock temperature.

REFERENCES

Aizu, K., 1973. Prog. Theor. Phys., 49, 1184
Arnaud, M., Rothenflug, R., 1985, A&AS, 60, 425
Bates, D. R., Kingston, A. E., McWhirter, R. E. P., 1962, Proc. Roy. Soc., A267, 297
Beardmore, A. P., Osborne, J. P., Hellier, C., 2000, MNRAS, 315, 307
Castor, J. I., 1993, in "UV and X-ray Spectroscopy of Laboratory and Astrophysical Plasmas", eds. E. Silver and S. Kahn, Cambridge University Press, Cambridge, p.69
Cropper, M., Ramsay, G., Wu, K., 1998, MNRAS, 293, 222
Cropper, M., Wu, K., Ramsay, G., 1999, in "Annapolis Workshop on Magnetic Cataclysmic Variables", eds. C. Hellier and K. Mukai, ASP Conf. Ser., 157, 325
Cropper, M., Wu, K., Ramsay, G., Kicabiyik, A., 1999, MNRAS, 306, 684
Elwert, G., 1952, Z. Naturf., 7a, 432
Ezuka, H., Ishida, M., 1999, ApJS, 120, 277
Fujimoto, R., 1996, PhD Thesis, University of Tokyo
Fujimoto, R., Ishida, M., 1995, in "Cape Workshop on Magnetic Cataclysmic Variables", eds. D. A. H. Buckley and B. Warner, ASP Conf. Ser., 85, 136
Fujimoto, R., Ishida, M., 1997, ApJ, 474, 774
Gorenstein, P., Harnden, R., Tucker, W., 1974, ApJ, 192, 661
Hellier, C., Mukai, K., Ishida, M., Fujimoto, R., 1996, MNRAS, 280, 877
Imamura, J. N., Durisen, R. H., Lamb, D. Q., Weast, G. J., 1987, ApJ, 313, 298

Ishida, M., 1991, PhD Thesis, University of Tokyo

Ishida, M., Matsuzaki, K., Fujimoto, R., Mukai, K., Osborne, J. P., 1997, MNRAS, 287, 651

Jacobs, V. L., Davis, J., Kepple, P. C., Blaha, M., 1977, ApJ, 211, 605

Jordan, C., 1969, MNRAS, 142, 501

Kahn, S. M., Liedahl, D. A., 1991, in "Iron Line Diagnostics in X-ray Sources", eds. A. Treves, G. C. Perola and L. Stella, Springer-Verlag, Berlin, p.3

Kallman, T. R., McCray, R., 1982, ApJS, 50, 263

Kato, T., 1976, ApJS, 30, 397

King, A. R., Lasota, J. P., 1979, MNRAS, 188, 653

Kylafis, N. D., Lamb, D. Q., 1982, ApJS, 48, 239

Lamb, D. Q., Masters, A. R., 1979, ApJ, 234, L117

Langer, S. H., Chanmugam, G., Shaviv, G., 1982, ApJ, 258, 289

Makishima, K., 1986, in "The Physics of Accretion onto Compact Objects", eds. K. O. Mason, M. G. Watson and N. E. White, Springer-Verlag, Berlin, p.249

Masai, K., 1984, APSS, 98, 367

Mewe, R., 1990, in "Physical Process in Hot Cosmic Plasmas", eds. W. Brinkmann, A. C. Fabian and F. Giovannelli, NATO ASI series, Kluwer, Dordrecht, p.39

Mewe, R., Gronenschild, E. H. B. M., 1981, A&AS, 45, 11

Mewe, R., Gronenschild, E. H. B. M., van den Oord, G. H. J., 1985, A&AS, 45, 11

Nauenberg, M., 1972, ApJ, 175, 417

Ramsay, G., Mason, K. O., Cropper, M., Watson, M. G., Clayton, K. L., 1994, MNRAS, 270, 692

Ramsay, G., 2000, MNRAS, 314, 403

Raymond, J. C., Smith, B. W., 1977, ApJS, 35 419

Rothschild, R. E. et al., 1981, ApJ, 250, 723

Saxton, C. J., 1999, PhD Thesis, University of Sydney

Saxton, C. J., Wu, K., 1999, MNRAS, 310, 677

Tennant, A. F., Wu, K., O'Dell, S. L., Weisskopf, M. C., 1998, Publ. Astr. Soc. Aus., 15, 339

Warner, B., 1995, Cataclysmic Variable Stars, Cambridge University Press, Cambridge

Wilson, R., 1962, Quant. Spectr. Rad. Transf., 2, 477

Wu, K., 1994, Proc. Astr. Soc. Aus., 11, 61

Wu, K., 2000, Sp. Sci. Rev., 93, 611

Wu, K., Chanmugam, G. & Shaviv, G., 1994, ApJ, 426, 664